Geophysical Research Letters

RESEARCH LETTER
10.1029/2019GL083282

Satellite Data-Based 3-D Simulation of Kelvin-Helmholtz Instability and Induced Magnetic Reconnection at the Earth's Magnetopause

M. Sisti[1,2], M. Faganello[1], F. Califano[2], and B. Lavraud[3]

[1]Aix-Marseille University, CNRS, PIIM UMR 7345, Marseille, France, [2]Physics Department, University of Pisa, Pisa, Italy, [3]IRAP, University of Toulouse, Toulouse, France

Key Points:
- We present a 3-D two-fluid simulation using plasma parameters as measured by MMS on 8 September 2015
- We observe that (Kelvin-Helmholtz) vortex induced and midlatitude magnetic reconnection coexist and cooperate
- We estimate the effective diffusion associated with reconnection, obtaining $D_{\text{eff}} \simeq 10^{10}\, m^2/s$, large enough to explain the observed mixing

Supporting Information:
- Supporting Information S1

Correspondence to:
M. Faganello,
matteo.faganello@univ-amu.fr

Citation:
Sisti, M., Faganello, M., Califano, F., & Lavraud, B. (2019). Satellite data-based 3-D simulation of Kelvin-Helmholtz instability and induced magnetic reconnection at the Earth's magnetopause. *Geophysical Research Letters*, *46*. https://doi.org/10.1029/2019GL083282

Received 24 APR 2019
Accepted 21 SEP 2019
Accepted article online 28 OCT 2019

Abstract We present a 3-D two-fluid simulation using plasma parameters as measured by MMS on 8 September 2015 concerning the nonlinear development of the Kelvin-Helmholtz instability at the Earth's magnetopause. We observe an extremely rich nonlinear dynamics including the development of a complex magnetic topology, vortex merging, and secondary Kelvin-Helmholtz instability driven by large-scale vortices distributed asymmetrically in latitude. Vortex induced and midlatitude magnetic reconnection coexist and produce an asymmetric distribution of magnetic reconnection events. These results are in good agreement with MMS observations on the same day, in particular for the presence of both equatorial and off-equator reconnection. Regarding the latter only, we note a predominance of reconnection in the Southern Hemisphere during the early nonlinear phase. The estimated effective diffusion coefficient associated with the dynamics is found to be large enough to account for the observed mass transport at the Earth's magnetospheric flanks.

1. Introduction

Several decades of studies definitely proved the key role played by the Kelvin-Helmholtz instability (KHI) in regulating plasma transport from the solar wind (SW) into planetary magnetospheres. In particular, satellite data collected around the Earth's magnetopause revealed the presence of rolled-up KH vortices (Hasegawa et al., 2004) under a variety of SW magnetic field orientations (Hasegawa et al., 2006; Hwang et al., 2011; Farrugia et al., 2014; Kavosi & Raeder, 2015) and the direct proof of magnetic reconnection events forced by the vortices themselves (Eriksson et al., 2016; Hasegawa et al., 2009). This proof is of paramount importance since KH vortices alone cannot explain the observed transport. Vortices develop as large-scale, nearly magnetohydrodynamic (MHD) structures that strongly perturb and fold the magnetopause but preserve the magnetic topology. Thus, they cannot induce an effective transport (Foullon et al., 2008; Nykyri & Otto, 2001). In contrast, new open field lines emerging from reconnection events allow particles to stream from the SW into the magnetosphere leading to direct plasma entry (Daughton et al., 2014; Nakamura & Daughton, 2014). This kind of dynamics is of great interest also for planetary magnetospheres (Johnson et al., 2014) and magnetized astrophysical objects characterized by the presence of strong velocity gradients (Li & Narayan, 2004; Lovelace et al., 2010). Here we focus our analysis on northward interplanetary magnetic field (IMF) periods at Earth when the magnetic field advected by the SW is mainly parallel to the magnetospheric one at low latitude but including a rotation in the transition from the SW to the magnetosphere. In this region KH vortices can effectively grow with wavevectors nearly perpendicular to the average magnetic field minimizing the effect of magnetic tension but still fairly aligned with the flowing SW maximizing the velocity shear driver (Faganello & Califano, 2017; Miura & Pritchett, 1982; Southwood, 1968; Walker, 1981). If an initial magnetic rotation is taken into consideration, the associated current sheet is pinched in between vortices, and Type I vortex induced reconnection (VIR) is forced on the ideal KH time scale, faster than the usual reconnection one (Chen & Morrison, 1990; Knoll & Chacón, 2002). VIR creates “open” field lines crossing the magnetopause eventually producing the development of a mixing layer (Nakamura et al., 2013). At magnetopause flanks, the KHI is gradually stabilized at higher latitudes (Contin, 2003; Farrugia et al., 1998; Gratton et al., 2003). As a result, magnetic field lines are advected differently at low latitude, once engulfed in vortices, and at high latitudes where the flow is more and more unperturbed. In such a way, even if IMF and magnetospheric field lines are aligned so that no magnetic rotation is present, midlatitude current sheets are created where reconnection finally occurs (Borgogno et al., 2015; Faganello et al., 2012). Proceeding at

the same time in both hemispheres, midlatitude reconnection (MLR) is able to create twice-reconnected, "newly closed" field lines connected to the Earth at both poles while embedded within SW plasma at low latitude. Twice-reconnected field lines allow for a direct and effective injection of SW plasma into the magnetosphere (Faganello et al., 2012; Johnson & Wing, 2009). Measurements of *remote* reconnection signatures using electron particle fluxes have been reported by Cluster (Bavassano Cattaneo et al., 2010), THEMIS (Faganello et al., 2014), and MMS Vernisse et al. (2016). In these works the location of reconnection sites is inferred by looking at the angle of detected suprathermal particles with respect to local magnetic field: Parallel particle fluxes are related to events occurring in the Southern Hemisphere, while antiparallel fluxes come from events in the northern one. Interestingly, MMS observations on 8 September 2015 indicate that VIR proceeding at equatorial latitude and MLR coexist (Eriksson et al., 2016; Vernisse et al., 2016). MMS was located close to the geocentric solar ecliptic (GSE) equatorial plane where vortices and in situ VIR outflows were detected. At the same time, satellites observed parallel and antiparallel particle fluxes as signatures of remote reconnection, with more events with parallel fluxes. This fact suggests that the latitudinal distribution of remote reconnection events was asymmetric, with more events located in the Southern Hemisphere rather than in the northern one. This dynamics have been confirmed by numerical simulations taking into account high-latitude stabilization as well as the initial magnetic rotation (Fadanelli et al., 2018) but not the actual magnetic/plasma parameters of the observed MMS event. The magnetic rotation breaks the reflection symmetry with respect the equatorial plane so that the system evolves differently in the two hemispheres. As a consequence, MLR and the production of twice-reconnected lines could be affected (Fadanelli et al., 2018; Ma et al., 2017). At the same time, local kinetic simulations of this MMS event have been performed focusing on VIR only (Nakamura, Eriksson, et al., 2017; Nakamura, Hasegawa, et al., 2017), showing that VIR can become turbulent producing a layer where different particle populations are effectively mixed up, with a local entry rate comparable with that required for the observed mass transfer during northward IMF periods (Sonnerup, 1980). However, for such simulations, the numerical box has a limited size in latitude; thus, they cannot reproduce the remote dynamics of MLR.

Here we analyze a 3-D two-fluid simulation using the parameters measured during the MMS event of 8 September 2015 and a large enough numerical box in order to include high-latitude stabilization. We show, in agreement with MMS observations, that VIR and MLR coexist and determine the complex magnetic field topology. To summarize, (i) even if the symmetry of MLR is broken by the presence of the large-scale magnetic field rotation, the production of twice-reconnected field lines is still efficient; (ii) the effective diffusion coefficient associated with such a complex topology can explain the observed transport in a wide latitude range; (iii) the asymmetry of reconnection events reproduces that observed during the MMS event on which the simulation parameters are set; and (iv) the late nonlinear phase is extremely rich with vortex merging and the development of secondary KH instability that boost the production of reconnected lines and the effective diffusivity. Our simulation is able to account for the main features characterizing the dynamics as inferred from MMS data on 8 September 2015 (Eriksson et al., 2016; Vernisse et al., 2016) and predicts an even more complex evolution of the magnetic topology when moving tailward as compared to the satellite position.

2. Plasma Model and Simulation Setup

We consider a slab geometry with the x axis perpendicular to the magnetopause, z as the latitude, and the y axis along the SW flow. The plasma evolution is described by a two-fluid set of equations:

$$\partial_t n + \nabla \cdot (n\mathbf{U}) = 0 \quad ; \quad n = n_\mathrm{i} \simeq n_\mathrm{e}, \tag{1}$$

$$\partial_t (n\mathbf{U}) + \nabla \cdot \left[n\mathbf{U}\mathbf{U} + (P_\mathrm{i} + P_\mathrm{e} + B^2/2)\bar{\bar{\mathbf{I}}} - \mathrm{BB} \right] = 0, \tag{2}$$

$$\partial_t (nS_j) + \nabla \cdot (nS_j \mathbf{u}_j) = 0 \quad ; \quad S_j = P_j n^{-5/3} \quad ; \quad j = i, e, \tag{3}$$

where n is the plasma density, $\mathbf{u}_\mathrm{i} \simeq \mathbf{U}$ the ion fluid velocity, $\mathbf{u}_\mathrm{e} = \mathbf{U} - \mathbf{J}/n$ the electron fluid velocity, $\mathbf{J} = \nabla \times \mathbf{B}$ the current density, and $P_j, j = i, e$ the pressures. All quantities are normalized using the ion mass

and charge, the ion skin depth d_i and the z component of the Alfvén velocity at the center of the simulation domain. The Faraday equation and a generalized Ohm's law

$$\mathbf{E} = -\mathbf{u}_e \times \mathbf{B} - \frac{1}{n}\nabla P_e + \eta \mathbf{J} \tag{4}$$

complete the set. We use a small but finite resitivity $\eta = 10^{-3}$, corresponding to a resistive diffusion time scale $\tau_R \simeq \eta^{-1}a^2 \simeq 10^4$, associated with the equilibrium-scale length a, which is far bigger than the simulation time. As a consequence, the magnetic field is frozen-in to the large-scale KH motion, and we do not observe any appreciable magnetic diffusion until reconnection starts in d_i-scale current sheets. Here reconnection is expected to develop on a time scale nearly independent of the η value as for Hall-dominated reconnection Birn et al. (2001). Even if a kinetic model would better reproduce the finer structures of magnetic reconnection, our description is nevertheless able to capture the correct reconnection time scale in the complex 3-D evolution of KHI and to describe the evolution of the global magnetic topology (Faganello et al., 2012). We model the initial large-scale configuration by using a 2-D Grad-Shafranov equilibrium that includes the strong gradients across the magnetopause and reproduces the high-latitude stabilization along z (Faganello et al., 2012). All equilibrium quantities are obtained by a flux function

$$\psi(x, z, t = 0) = \frac{2}{3}x + \frac{1}{3}\frac{L_z}{2\pi}\sinh\frac{2\pi x}{Lz}\cos\frac{2\pi z}{L_z}, \tag{5}$$

giving $\mathbf{B}_{eq} = \nabla\psi \times \hat{y}l + (B_{flow}/2)[1 + \tanh(\psi/a)]\hat{y}$, $n_{eq} = 1 + (\Delta n/2)\tanh(\psi/a)$, $\mathbf{U}_{eq} = (\Delta U/2)\tanh(\psi/a)\hat{y}$, $P_{i,eq} + P_{e,eq} + B^2_{eq,y}/2 = (P_{i,eq} + P_{e,eq} + B^2_{eq,y}/2)|_{\psi=0}$ with $P_{i,eq} = 4P_{e,eq}$. Here B_{flow} is the flow-aligned component of the IMF that, adding to the northward component of the magnetic field, reproduces its rotation. We take equilibrium quantities compatible with the MMS event, as given by the values reported in the outer magnetosphere and in the adjacent magnetosheath in the auxiliary material of Eriksson et al. (2016). In particular ,n varies from 5.7 to 20.1 cm^{-3}, with an averaged value of ∼13 cm^{-3}. Using this value when normalizing, we have $n = 1$ at the magnetopause and $\Delta n = 1$. The GSE z component of the magnetic field is nearly constant at ∼67 nT, while the flow-aligned component in the sheath is approximately − 24 nT. The velocity jump is ∼350 km/s. As a consequence, normalized quantities read $B_{z,eq}|_{\psi=0} = 1$, $B_{flow} = -0.3$ and $\Delta U = 0.9$. The thermal temperature varies from $T_{th} = T_i + T_e = 2,638\,\text{eV} + 124\,\text{eV} \sim 2,800\,\text{eV}$ to $T_{th} = T_i + T_e = 189\,\text{eV} + 36\,\text{eV} \sim 200\,\text{eV}$; thus, the averaged thermal temperature is ∼1,500 eV and $(P_{i,eq} + P_{e,eq})|_{\psi=0} = 0.9$. The pressure equilibrium condition given above reproduces a temperature jump across the magnetopause of ∼2,080 eV, slightly less but consistent with the MMS data. We set $a = 3$ so that the fastest growing mode (FGM) wavelength $\lambda_{FGM} \simeq 4\pi a$ is big as compared to d_i and KH vortices develop at MHD scales. The box size is given by $L_x = 90 \simeq 2.4\lambda_{FGM}$, $L_y = 24\pi = 2\lambda_{FGM}$, and $L_z = 96\pi = 8\lambda_{FGM}$. The number of grid points is $n_x = 600$ and $n_y = n_z = 512$. All details on the numerical code, including transparent boundary conditions, can be found in Fadanelli et al. (2018) and references therein.

3. Data Analysis

In Figure 1a, we show a 3-D rendering of the KH vortices at $t = 525$. Vortices develop around the equator, while high-latitude regions are stable. The vortex axis, as shown by the folded shaded surface of the magnetopause, is tilted with respect to $\hat{z}$ since the FGM wavevector is nearly perpendicular to the average $\mathbf{B}_{eq}$ in the central region. This tilting is also underlined by the three central planes drawn perpendicularly to the vortex axis. As expected for $B_{flow} < 0$ (Fadanelli et al., 2018), vortices are more intense above the equatorial plane since the differential advection of field lines enhances the magnetic rotation in the Southern Hemisphere and lower it in the northern one. Indeed, as shown in Figure 1b, $max_{(x,y)}(|J_\parallel|)$ (the maximum is searched in the entire xy plane) as a function of z becomes larger and larger in the Southern Hemisphere (here $J_\parallel = \mathbf{J}\cdot\mathbf{B}/|\mathbf{B}|$). Since the presence of a magnetic rotation tends to stabilize the KHI (see Figure 1b), the vortices are favored above $z = 0$ (Figure 1c) where $max_{(x,y)}(u_{ix})$ is larger in the Northern Hemisphere. Figures 1d–1f show density isocountours at different stages of the vortex evolution above the equator (at $z = 68$, close to the latitude where the vortices are more intense): at $t = 500$ when vortices are fully rolled up; at $t = 600$ when they start to merge (Miura, 1997); and at $t = 725$ when a single large-scale vortex has formed, while small-scale secondary KHI (Matsumoto & Hoshino, 2004; Smyth, 2003) develops at the low-density boundary of the vortex where strong velocity gradients exists. At $z = -30$ (where the current peaks), KH nonlinear evolution proceeds in similar way (slightly less intense rolled-up vortices that finally merge), but no sign of secondary KHI appears, probably due to the enhanced magnetic shear. The evolution

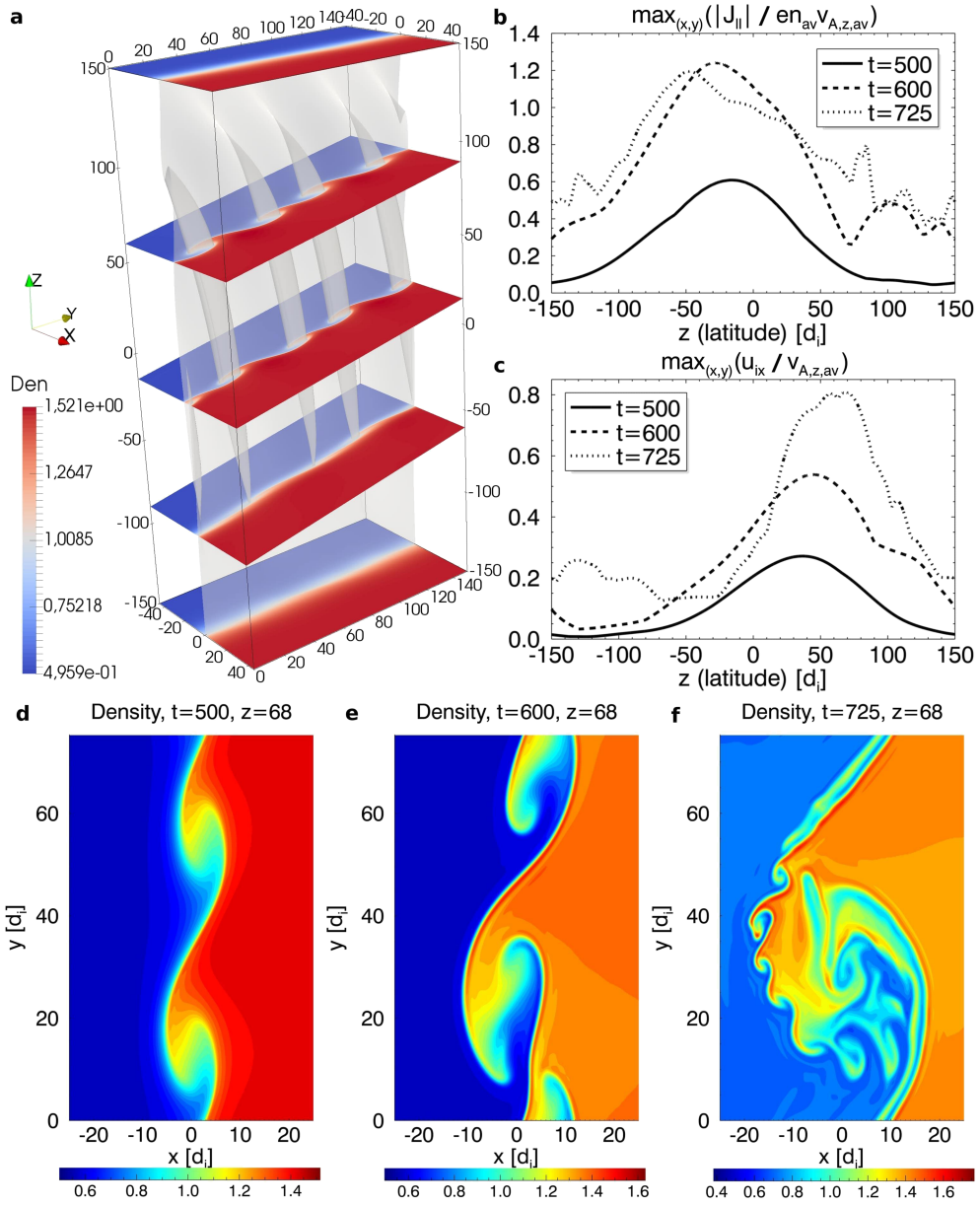

Figure 1. (a) 3-D rendering of Kelvin-Helmholtz vortices at $t = 525$. Blue and red colors represent plasma density (red = high density; blue = low density). The gray shaded surface, $\psi = 0$, corresponds to the magnetopause. The three central planes are perpendicular to the vortex axis. The box has been doubled along y direction for sake of clearness. (b,c) Plot of $max_{(x,y)}(|J_{\|}|)$ and of $max_{(x,y)}(u_{ix})$ as a function of z at $t = 500$ (dashed), $t = 600$ (dotted), $t = 725$ (continuous). (d–f) Density iso-contours at the latitude $z = 68$ for three different times $t = 500$, $t = 600$, and $t = 725$.

of $|J_{\|}|$ suggests that VIR should occur close to the equatorial plane at $t \sim 500$ where a single broad current peak is generated by the vortex pinching of the initial current sheet(see Figure 1b, continuous line). Later on, at $t = 600$, a secondary current peak is visible at $z \sim 100$ so that MLR is expected to occur in the Northern Hemisphere (dashed line), while the main broad peak, although shifted southward by differential advection, would remain linked to VIR. Since reconnection in a 3-D geometry is not trivial to be identified, we follow the ideal MHD evolution of the initial magnetic surfaces by integrating in time $\partial_t \psi + \mathbf{U} \cdot \nabla \psi = 0$. At $t = 0$, $|\psi|$ measures the distance from the (perturbed) magnetopause, with $\psi \simeq x$ around $z = 0$.

To look at reconnected field lines, we trace at given times a set of 22,500 magnetic field lines whose feet are uniformly distributed in the (x, y) region $[-15, 15] \times [0, L_y]$ at $z = -L_z/2$. We define a line as "reconnected" when ψ has a jump along the line of at least $\pm a/2$ across the magnetopause. "Once-reconnected" lines have

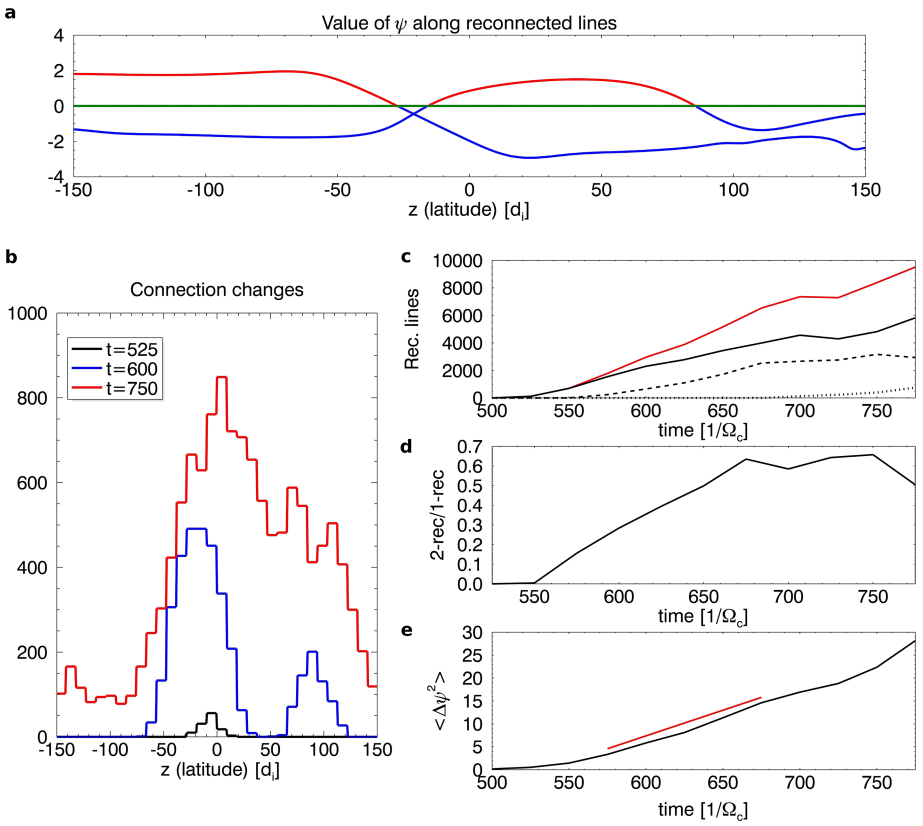

Figure 2. (a) ψ as a function of z for two chosen magnetic field lines at $t = 600$. Blue and red colors are set according to the plasma lines are connected to. The green line represents the magnetopause. (b) Latitudinal distribution of connection changes at $t = 525$ (black), $t = 600$ (blue), and, finally, $t = 750$ (red). (c) Time evolution of the total number of reconnected field lines (red), once (black), twice (black dashed), and 2^+-reconnected (black dotted) lines. (d) Time evolution of the ratio between twice-reconnected and once-reconnected lines. (e) Time evolution of $< \Delta\psi^2 >$, the slope 0.1 (red) is given as reference.

only one jump, "twice-reconnected" lines have two jumps, and we call "2^+-reconnected" lines with three or more jumps. In order to provide a visual representation of the previous definitions, in Figure 2a, we plot the value of ψ along two chosen magnetic field lines. One is once-reconnected and has a single ψ jump around $z \lesssim 0$, while the other is twice-reconnected having a second jump around $z \sim 100$. Note that around both latitudes, where the connection changes occur, we observe clear ion and electron outflows pointing away from the site where the parallel current is maximal and where reconnection is proceeding (see Figures S1 and S2 in the supporting information). Signatures of the Hall quadrupole are visible below $z = 0$, even if quite distorted because of the "guide field" effect (Eastwood et al., 2010) and of the density asymmetry across the current sheet (Pritchett, 2008). A kinetic description would probably reduce the distortion associated with the density asymmetry since particles streaming along reconnected field lines would rapidly smooth out density variations (Sturner et al., 2018). At $z \sim 100$, the magnetic fluctuations due to the KH vortex strengthen, suppressing possible quadrupolar signatures (see Figures S3 and S4).

For all field lines having a jump in ψ, we record the latitude at which they cross the magnetopause in order to obtain a latitudinal distribution of sites of connection changes (Figure 2b). At $t = 525$, this distribution is peaked just below $z = 0$ where VIR has created once-reconnected field lines. At $t = 600$, a second bump around $z \sim 100$ is present corresponding to lines having reconnected a second time in the northern current peak due to MLR. The main peak associated with VIR has moved southward, as the main current peak did. These dynamics are confirmed by the temporal evolution of the number of once- or twice-reconnected lines (see Figure 2c). At the beginning, only once-reconnected lines are present, and their number increases in time. After a while, they reconnect a second time at midlatitude (in correspondence of the northern current peak, not shown), and the number of twice-reconnected lines increases too. The ratio between once-

Table 1
Number of In Situ and Remote Events

Time interval	Southern h.	In situ	Northern h.
501–525	35	81	2
526–550	377	201	7
551–575	677	321	327
576–600	730	268	590
601–625	544	145	686
626–650	694	247	953
651–675	488	356	1346
676–700	147	328	747
701–725	—	120	757
726–750	650	—	1656

and twice-reconnected lines slowly increases in time (Figure 2d) until $t \sim 675$ suggesting that the dynamics favor an efficient conversion from once- to twice-reconnected lines. After $t \sim 675$, this ratio reaches a plateau corresponding to nearly 60% of twice-reconnected lines. Even if not all once-reconnected lines reconnect a second time, the number of lines doing this is far from being negligible. The production rate of twice-reconnected line is smaller by a factor of 3 than in the case without an initial magnetic rotation (Borgogno et al., 2015) but is of the same order of magnitude. The number of 2^+-reconnected lines stays negligible.

Reconnection leads to the development of a mixing layer across the magnetopause where field lines have different topologies, from the original one, to "open" connection and newly closed ones. Because the mixing between the different populations is dominated by parallel streaming along reconnected lines (Daughton et al., 2014; Nakamura et al., 2013), in our fluid approach, we look at the average displacement of magnetic field lines with respect to their initial distance from the magnetopause. We thus evaluate $< \Delta\psi^2 >$, where the average is on the set of 22,500 field lines defined above, $\Delta\psi = max(\psi) - min(\psi)$ along a line and where $\sqrt{< \Delta\psi^2 >}$ would thus correspond to the average width of the mixing layer. As shown in Figure 2e, $< \Delta\psi^2 >$ grows linearly in time from $t \simeq 575$ to $t \simeq 675$, indicating a diffusive-type widening of the mixing layer, with an effective magnetic and matter diffusion coefficient $D_{\text{eff}} \simeq 0.1 v_{A,z} d_i$. Taking a z component of the Alfvén velocity $v_{A,z} \simeq 400$ km/s and $d_i \simeq 300$ km (which corresponds to a KH wavelength $\lambda_{KH} \simeq 12,000$ km, as inferred in the MMS event) , we obtain $D_{\text{eff}} \simeq 10^{10}\,\text{m}^2/\text{s}$, even bigger than the diffusion coefficient needed to account for the observed plasma mixing in a simplified viscous model of the magnetopause (Sonnerup, 1980).

Since all new connection changes observed during a given time interval are due to reconnection events, we can compare the spatial distribution of reconnection sites obtained in our simulation with the ones inferred during the MMS event (Vernisse et al., 2016). In order to reproduce a magnetopause crossing by a virtual satellite at equatorial latitudes, we define three cases: (1) in situ reconnection sites (with respect to the MMS spacecraft position) when the magnetopause crossing is located around the equators ($-10\,d_i < z < +10\,d_i$); (2) remote sites in the Northern Hemisphere for a crossing at $z > +10 d_i$; and (3) remote sites in the Southern Hemisphere for a crossing at $z < -10\,d_i$. These definitions are related to the satellite position, not to the type of reconnection going on. The results for different time intervals are listed in Table 1. In agreement with the MMS event (Vernisse et al., 2016) in the early nonlinear phase ($t \lesssim 600$), the most of the remote reconnection sites are located in the southern rather than in the Northern Hemisphere. Note that vortices are expected to be in their early nonlinear phase for this event, as inferred by Nakamura, Hasegawa, et al. (2017) by a careful comparison between their local simulation and the MMS observations. Moreover, MMS satellites are close to the GSE equatorial plane (Eriksson et al., 2016), where the growth rate of the KHI is supposed to be close to its maximum (Vernisse et al., 2016). In our case, this plane correspond to the $z = 0$ one.

In order to interpret the complex topology extrapolated from MMS data, in Figure 3, we draw the density iso-contours corresponding to a 2-D chart of vortices in the equatorial plane during the early nonlinear phase, together with the intersection points of reconnected field lines. At $t = 550$, black circles symbolize once-reconnected lines, generated by VIR. These lines intersect the selected plane close to the compressed

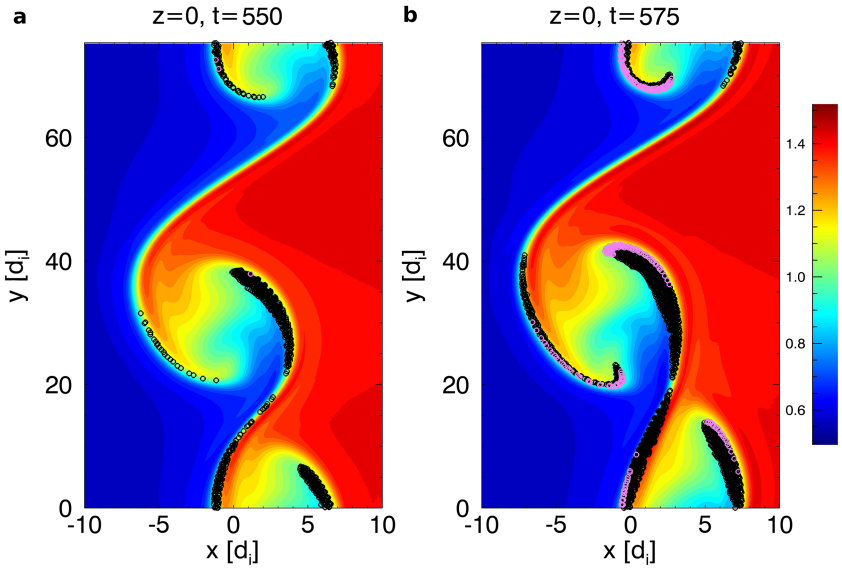

Figure 3. Density iso-contours at $z = 0$ (red = high density; blue = low density) and positions of the intersection points of the reconnected field lines in the equatorial plane ($z = 0$) at $t = 550$ (a) and $t = 575$ (b). Black denotes once-reconnected lines, and purple denotes twice-reconnected ones.

current sheet between vortices. The number of these intersection points gradually increases in time along the vortex arms. An "arm" is defined as the low (high) density plasma plume that is gradually folded into a vortex, for example, the blue (red) region in between $y \sim 20$ and $y \sim 40$, at $x \sim 2$ ($x \sim -5$). Since these lines reconnect at $z \lesssim 0$, satellites at $z \simeq 0$ would measure either in situ reconnection signatures, for example, reconnection outflows and Hall magnetic field, or accelerated particles streaming parallel to **B** (coming from the south). It is worth noticing that due to the relative motion of vortices during their merging, the current sheet centered at $y \sim 20$ is more compressed and enhanced as compared to the one in $y \sim 55$. At later times, $t = 575$, some field lines have also reconnected a second time also in the Northern Hemisphere (purple points) and satellites encountering these twice-reconnected field lines would also observe also antiparallel particle fluxes. Note that black intersection points are located either close to the compressed current sheet or along vortex arms, while purple points are only located along vortex arms. This kind of behavior associated with remote MLR, for which antiparallel fluxes of accelerated particles from northern reconnection sites could be detected only along the vortex arms, could help in discerning this type of reconnection mechanism from other kinds of remote reconnection events, such as lobe reconnection (Gosling et al., 1991; Le et al., 1994; Song & Russell, 1992), for which the intersection points would be equally distributed between the compressed current sheet and the vortex arms.

In the late nonlinear phase, vortices first merge ($t \simeq 600$), and then the single large vortex turns out to be unstable with respect to secondary KHI ($t \simeq 700$) that develops at latitudes around $z \simeq 70$. During vortex merging, the increase of reconnected lines is slightly slowed down (Figure 2c), while more events are recorded in the Northern Hemisphere than in the southern one (see Table 1). When, for $t \simeq 700$, secondary KHI grows along the vortex SW arm around $z \simeq 70$, it forces reconnection to occur and boosts the production of reconnected lines. As a consequence, the latitude distribution of reconnection sites changes from a two-bump structure (Figure 2b, blue line) to a single wider distribution (Figure 2b, red line) with lots of magnetopause crossings from $z \simeq -70$ to $z \simeq 130$.

4. Discussion and Summary

By performing a 3-D two-fluid simulation using the parameters measured by MMS on 8 September 2015 and using a large numerical box including high-latitude stabilization, we have studied the development remote northern MLR together with VIR. Even if the North-South symmetry of the system is broken, the production of twice-reconnected lines turns out to be fairly efficient with 60% of once-reconnected lines reconnecting a second time. An estimation of the diffusion coefficient D_{eff} associated with reconnection turns out to be large enough to explain the observed plasma mixing (Sonnerup, 1980) and compatible with the one inferred

by Nakamura, Eriksson, et al. (2017) and Nakamura, Hasegawa, et al. (2017) where, however, the numerical box is too small to account for the remote dynamics. Two main regimes have been identified thanks to the analysis of connection changes. In the early nonlinear phase, VIR and northern MLR coexist and generate a latitudinal distribution of connection changes with two different bumps at different latitudes. Following a virtual satellite around the equatorial plane, we observe, as found by MMS, more "remote" events in the Southern Hemisphere than in the northern. However, while Vernisse et al. (2016) identify southern remote events as MLR, our simulation suggests that they could be related to VIR, which is found to develop in a wide latitude range reaching into the Southern Hemisphere.

In the late nonlinear phase, as it would be observed by satellites farther tailward along the magnetopause, vortex merging and secondary KHI develop and force reconnection to occur in a wider latitudinal range. In this case the number of reconnection events becomes larger in the Northern Hemisphere. Finally, we show a 2-D chart of KH vortices in the equatorial plane with reconnection line intersections that would help in discerning MLR from other kinds of remote reconnection events in observations. Indeed, during the early nonlinear phase, particles signatures from remote MLR is limited in space along the vortex arms, while particle signatures from lobe reconnection would intersect the entire mixing region uniformly.

Acknowledgments
The simulation data are stored in the PIIM laboratory repository and are available online (https://storagepiim.etoile.univ-amu.fr/share.cgi?ssid=00SbRzp).

References

Bavassano Cattaneo, M. B., Marcucci, M. F., Bogdanova, Y. V., Rème, H., Dandouras, I., Kistler, L. M., & Lucek, E. (2010). Global reconnection topology as inferred from plasma observations inside Kelvin-Helmholtz vortices. *Annales Geophysicae*, *28*(4), 893–906.

Birn, J., Drake, J. F., Shay, M. A., Rogers, B. N., Denton, R. E., Hesse, M., et al. (2001). Geospace Environmental Modeling (GEM) Magnetic Reconnection Challenge. *Journal of Geophysical Research*, *106*(A3), 3715–3719.

Borgogno, D., Califano, F., Faganello, M., & Pegoraro, F. (2015). Double-reconnected magnetic structures driven by Kelvin-Helmholtz vortices at the Earth's magnetosphere. *Physics of Plasmas*, *22*(3), 032301. https://doi.org/10.1063/1.4913578

Chen, X. L., & Morrison, P. J. (1990). Resistive tearing instability with equilibrium shear flow. *Physics of Fluids B: Plasma Physics*, *2*(3), 495–507. https://doi.org/10.1063/1.859339

Contin, J. E. (2003). Theoretical results on the latitude dependence of the Kelvin-Helmholtz instability at the dayside magnetopause for northward interplanetary magnetic fields. *Journal of Geophysical Research*, *108*(A6), 1227. https://doi.org/10.1029/2002JA009319

Daughton, W., Nakamura, T. K. M., Karimabadi, H., Roytershteyn, V., & Loring, B. (2014). Computing the reconnection rate in turbulent kinetic layers by using electron mixing to identify topology. *Physics of Plasmas*, *21*(5), 052307. https://doi.org/10.1063/1.4875730

Eastwood, J. P., Shay, M. A., Phan, T. D., & Øieroset, M. (2010). Asymmetry of the ion diffusion region hall electric and magnetic fields during guide field reconnection: Observations and comparison with simulations. *Physical Review Letters*, *104*, 205001. https://doi.org/10.1103/PhysRevLett.104.205001

Eriksson, S., Lavraud, B., Wilder, F. D., Stawarz, J. E., Giles, B. L., Burch, J. L., et al. (2016). Magnetospheric Multiscale observations of magnetic reconnection associated with Kelvin-Helmholtz waves. *Geophysical Research Letters*, *43*, 5606–5615.

Fadanelli, S., Faganello, M., Califano, F., Cerri, S. S., Pegoraro, F., & Lavraud, B. (2018). North-south asymmetric Kelvin-Helmholtz instability and induced reconnection at the Earth's magnetospheric flanks. *Journal of Geophysical Research: Space Physics*, *123*, 9340–9356. https://doi.org/10.1029/2018JA025626

Faganello, M., & Califano, F. (2017). Magnetized Kelvin–Helmholtz instability: Theory and simulations in the Earths magnetosphere context. *Journal of Plasma Physics*, *83*(6). https://doi.org/10.1017/S0022377817000770

Faganello, M., Califano, F., Pegoraro, F., & Andreussi, T. (2012). Double mid-latitude dynamical reconnection at the magnetopause: An efficient mechanism allowing solar wind to enter the Earth's magnetosphere. *EPL (Europhysics Letters)*, *100*(6), 69001. https://doi.org/10.1209/0295-5075/100/69001

Faganello, M., Califano, F., Pegoraro, F., Andreussi, T., & Benkadda, S. (2012). Magnetic reconnection and Kelvin-Helmholtz instabilities at the Earth's magnetopause. *Plasma Physics and Controlled Fusion*, *54*(12), 124037. https://doi.org/10.1088/0741-3335/54/12/124037

Faganello, M., Califano, F., Pegoraro, F., & Retinò, A. (2014). Kelvin-Helmholtz vortices and double mid-latitude reconnection at the Earth's magnetopause: Comparison between observations and simulations. *EPL (Europhysics Letters)*, *107*(1), 19001. https://doi.org/10.1209/0295-5075/107/19001

Farrugia, C. J., Gratton, F. T., Bender, L., Biernat, H. K., Erkaev, N. V., Quinn, J. M., et al. (1998). Charts of joint Kelvin-Helmholtz and Rayleigh-Taylor instabilites at the dayside magnetopause for strongly northward interplanetary magnetic field. *Journal of Geophysical Research*, *103*(A4), 6703–6727. https://doi.org/10.1029/97JA03248

Farrugia, C. J., Gratton, F. T., Gnavi, G., Torbert, R. B., & Wilson, L. B. (2014). A vortical dawn flank boundary layer for near-radial IMF: Wind observations on 24 October 2001. *Journal of Geophysical Research: Space Physics*, *119*, 4572–4590. https://doi.org/10.1002/2013JA019578

Foullon, C., Farrugia, C. J., Fazakerley, A. N., Owen, C. J., Gratton, F. T., & Torbert, R. B. (2008). Evolution of Kelvin-Helmholtz activity on the dusk flank magnetopause. *Journal of Geophysical Research*, *113*, A11203. https://doi.org/10.1029/2008JA013175

Gosling, J. T., Thomsen, M. F., Bame, S. J., Elphic, R. C., & Russell, C. T. (1991). Observations of reconnection of interplanetary and lobe magnetic field lines at the high-latitude magnetopause. *Journal of Geophysical Research*, *96*(A8), 14,097–14,106. https://doi.org/10.1029/91JA01139

Gratton, F. T., Gnavi, G., Farrugia, C. J., & Bender, L. (2003). The stability of the pristine magnetopause. *Planetary and Space Science*, *51*(12), 769–783. https://doi.org/10.1016/S0032-0633(03)00113-2

Hasegawa, H., Fujimoto, M., Phan, T.-D., Reme, H., Balogh, A., Dunlop, M. W., et al. (2004). Transport of solar wind into Earth's magnetosphere through rolled-up Kelvin-Helmholtz vortices. *Nature*, *430*(7001), 755. https://doi.org/10.1038/nature02799

Hasegawa, H., Fujimoto, M., Takagi, K., Saito, Y., Mukai, T., & RÃṁe, H. (2006). Single-spacecraft detection of rolled-up Kelvin-Helmholtz vortices at the flank magnetopause. *Journal of Geophysical Research*, *111*, A09203. https://doi.org/10.1029/2006JA011728

Hasegawa, H., Retinò, A., Vaivads, A., Khotyaintsev, Y., André, M., Nakamura, T. K. M., et al. (2009). Kelvin-Helmholtz waves at the Earth's magnetopause: Multiscale development and associated reconnection. *Journal of Geophysical Research*, *114*, A12207. https://doi.org/10.1029/2009JA014042

Hwang, K. J., Kuznetsova, M. M., Sahraoui, F., Goldstein, M. L., Lee, E., & Parks, G. K. (2011). Kelvin-Helmholtz waves under southward interplanetary magnetic field. *Journal of Geophysical Research*, *116*, A08210. https://doi.org/10.1029/2011JA016596

Johnson, J. R., & Wing, S. (2009). Northward interplanetary magnetic field plasma sheet entropies. *Journal of Geophysical Research*, *114*, A00D08. https://doi.org/10.1029/2008JA014017

Johnson, J. R., Wing, S., & Delamere, P. A. (2014). Kelvin Helmholtz instability in planetary magnetospheres. *Space Science Reviews*, *184*(1), 1–31. https://doi.org/10.1007/s11214-014-0085-z

Kavosi, S., & Raeder, J. (2015). Ubiquity of Kelvin-Helmholtz waves at Earth's magnetopause. *Nature Communications*, *6*, 7019. https://doi.org/10.1038/ncomms8019

Knoll, D. A., & Chacón, L. (2002). Magnetic reconnection in the two-dimensional Kelvin-Helmholtz instability. *Physical Review Letters*, *88*(21), 215003. https://doi.org/10.1103/PhysRevLett.88.215003

Le, G., Russell, C. T., & Gosling, J. T. (1994). Structure of the magnetopause for low Mach number and strongly northward interplanetary magnetic field. *Journal of Geophysical Research*, *99*(A12), 23,723–23,734. https://doi.org/10.1029/94JA02182

Li, L.-X., & Narayan, R. (2004). Quasi-periodic oscillations from Rayleigh-Taylor and Kelvin-Helmholtz instability at a disk-magnetosphere interface. *The Astrophysical Journal*, *601*(1), 414–427. https://doi.org/10.1086/380446

Lovelace, R. V. E., Romanova, M. M., & Newman, W. I. (2010). Kelvin-Helmholtz instability of the magnetopause of disc-accreting stars. *Monthly Notices of the Royal Astronomical Society*, *402*(4), 2575–2582. https://doi.org/10.1111/j.1365-2966.2009.16070.x

Ma, X., Delamere, P., Otto, A., & Burkholder, B. (2017). Plasma transport driven by the three-dimensional Kelvin-Helmholtz instability. *Journal of Geophysical Research: Space Physics*, *122*, 10,382–10,395. https://doi.org/10.1002/2017JA024394

Matsumoto, Y., & Hoshino, M. (2004). Onset of turbulence induced by a Kelvin-Helmholtz vortex. *Geophysical Research Letters*, *31*, L02807. https://doi.org/10.1029/2003GL018195

Miura, A. (1997). Compressible magnetohydrodynamic Kelvin-Helmholtz instability with vortex pairing in the two-dimensional transverse configuration. *Physics of Plasmas*, *4*(8), 2871–2885. https://doi.org/10.1063/1.872419

Miura, A., & Pritchett, P. L. (1982). Nonlocal stability analysis of the MHD Kelvin-Helmholtz instability in a compressible plasma. *Journal of Geophysical Research*, *87*(A9), 7431–7444. https://doi.org/10.1029/JA087iA09p07431

Nakamura, T. K. M., & Daughton, W. (2014). Turbulent plasma transport across the Earth's low-latitude boundary layer. *Geophysical Research Letters*, *41*, 8704–8712. https://doi.org/10.1002/2014GL061952

Nakamura, T. K. M., Daughton, W., Karimabadi, H., & Eriksson, S. (2013). Three-dimensional dynamics of vortex-induced reconnection and comparison with THEMIS observations. *Journal of Geophysical Research: Space Physics*, *118*, 5742–5757.

Nakamura, T. K. M., Eriksson, S., Hasegawa, H., Zenitani, S., Li, W. Y., Genestreti, K. J., et al. (2017). Mass and energy transfer across the Earth's magnetopause caused by vortex-induced reconnection. *Journal of Geophysical Research: Space Physics*, *122*, 11505–11522. https://doi.org/10.1002/2017JA024346

Nakamura, T. K. M., Hasegawa, H., Daughton, W., Eriksson, S., Li, W. Y., & Nakamura, R. (2017). Turbulent mass transfer caused by vortex induced reconnection in collisionless magnetospheric plasmas. *Nature Communications*, *8*(1), 1582. https://doi.org/10.1038/s41467-017-01579-0

Nykyri, K., & Otto, A. (2001). Plasma transport at the magnetospheric boundary due to reconnection in Kelvin-Helmholtz vortices. *Geophysical Research Letters*, *28*(18), 3565–3568. https://doi.org/10.1029/2001GL013239

Pritchett, L. P. (2008). Collisionless magnetic reconnection in an asymmetric current sheet. *Journal of Geophysical Research*, *113*, A06210. https://doi.org/10.1029/2007JA012930

Smyth, W. D. (2003). Secondary Kelvin-Helmholtz instability in weakly stratified shear flow. *Journal of Fluid Mechanics*, *497*, 67–98. https://doi.org/10.1017/S0022112003006591

Song, P., & Russell, C. T. (1992). Model of the formation of the low-latitude boundary layer for strongly northward interplanetary magnetic field. *Journal of Geophysical Research*, *97*(A2), 1411–1420. https://doi.org/10.1029/91JA02377

Sonnerup, B. U. Ö. (1980). Theory of the low-latitude boundary layer. *Journal of Geophysical Research*, *85*(A5), 2017–2026. https://doi.org/10.1029/JA085iA05p02017

Southwood, D. J. (1968). The hydromagnetic stability of the magnetospheric boundary. *Planetary and Space Science*, *16*(5), 587–605. https://doi.org/10.1016/0032-0633(68)90100-1

Sturner, A. P., Eriksson, S., Nakamura, T., Gershman, D. J., Plaschke, F., Ergun, R. E., et al. (2018). On multiple hall-like electron currents and tripolar guide magnetic field perturbations during Kelvin-Helmholtz waves. *Journal of Geophysical Research: Space Physics*, *123*, 1305–1324. https://doi.org/10.1002/2017JA024155

Vernisse, Y., Lavraud, B., Eriksson, S., Gershman, D. J., Dorelli, J., Pollock, C., et al. (2016). Signatures of complex magnetic topologies from multiple reconnection sites induced by Kelvin-Helmholtz instability. *Journal of Geophysical Research: Space Physics*, *121*, 9926–9939. https://doi.org/10.1002/2016JA023051

Walker, A. D. M. (1981). The Kelvin-Helmholtz instability in the low-latitude boundary layer. *Planetary and Space Science*, *29*(10), 1119–1133. https://doi.org/10.1016/0032-0633(81)90011-8